

Skymion lattice in centrosymmetric magnets with local Dzyaloshinsky-Moriya interaction

Shi-Zeng Lin^{1,2}

¹*Theoretical Division, T-4 and CNLS, Los Alamos National Laboratory,*

Los Alamos, New Mexico 87545, USA

²*Center for Integrated Nanotechnologies (CINT),*

Los Alamos National Laboratory, Los Alamos, New Mexico 87545, USA

(Dated: April 10, 2024)

Abstract

It is common for the local inversion symmetry to break in crystals, even though the whole crystal has global inversion symmetry. This local inversion symmetry breaking allows for a local Dzyaloshinsky-Moriya interaction (DMI) in magnetic crystals. Here we show that the local DMI can stabilize a skyrmion as a metastable excitation or as a skyrmion crystal in equilibrium. We consider the crystal structure with layered structure as an example, where local inversion is violated in each layer but a global inversion center exists in the middle of the two layers. These skyrmions come in pairs that are related by inversion symmetry. The two skyrmions with opposite helicity in a pair form a bound state. We study the properties of a skyrmion pair in the ferromagnetic background and determine the equilibrium phase diagram, where a robust lattice of skyrmion pairs is stabilized. Our results point to a new direction to search for the skyrmion lattice in centrosymmetric magnets.

I. INTRODUCTION

Magnetic skyrmions are topologically protected localized excitations, which have attracted considerable attention recently. [1–4] Skyrmions have many promising applications in spintronic devices because of their compact size, high mobility, and stability. Both single skyrmion and skyrmion lattice have been observed in a wide classes of magnetic materials, indicating their ubiquitous existence. This includes chiral magnets [5–8], magnetic multilayers [9, 10] and centrosymmetric magnets [11–13]. In chiral magnets and multilayers, the skyrmions are stabilized by the Dzyaloshinsky-Moriya interaction (DMI) [14–16] as a consequence of inversion symmetry breaking. [17–19] While in the centrosymmetric magnets, skyrmions are stabilized by frustrated or competing magnetic interactions. [20–22] Despite the tremendous progress in the past in identifying new skyrmion hosting materials, it is always demanding to find a new mechanism to stabilize skyrmions, as such a new mechanism will likely lead to novel physical properties of skyrmions, which may be desirable for device applications.

Here, we demonstrate that the DMI due to local inversion symmetry breaking in globally centrosymmetric magnets can also support skyrmions. Global centrosymmetry alone is not enough to forbid DMI. Instead, the inversion symmetry can be broken locally, which admits a local spin orbit coupling and hence DMI. One example is the spins in honeycomb lattice. Two nearest neighbor spins are inversion symmetric with the inversion center localized at the center of the bond, thus forbidding the DMI. However, there is no inversion symmetry for the two next-nearest-neighbor spins, and therefore a local DMI is allowed. The honeycomb lattice has mirror symmetry with respect to the honeycomb plane. As a result, the Moriya rule [15] dictates that the DMI vector is perpendicular to the honeycomb plane. Including such a DMI to the nearest-neighbor ferromagnetic Heisenberg model on the honeycomb lattice realizes a Haldane model for the magnons with topological magnon bands. [23]

II. MICROSCOPIC MODEL

To be specific, let us consider the crystal structure of type CaBe_2Ge_2 (space group 129, see Fig. 1 for a schematic view [24]). The magnetic ions (light orange) form a layered square lattice with odd and even layers, which are related by the inversion symmetry. Inside each layer, the local inversion symmetry is broken, which allows for a Rashba spin orbit interaction. The local

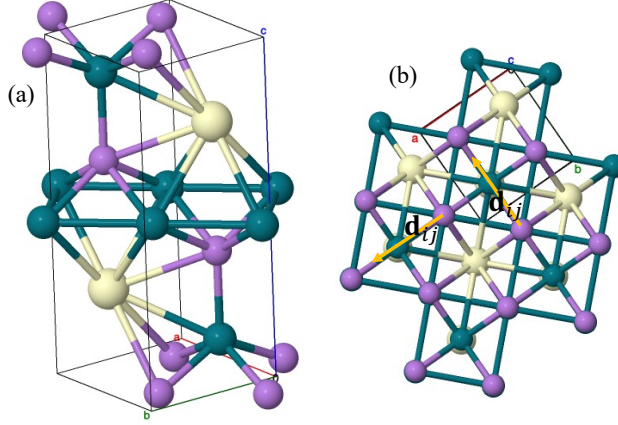


FIG. 1. (a) Unit cell of the crystal structure of type CaBe_2Ge_2 . We consider a material system with two magnetic ions (light orange sphere) in a unit cell. Each magnetic ion is not an inversion center, but the two magnetic ions are related by inversion with the inversion center located at the middle of the bond connecting these two ions. (b) Enlarged unit cell where magnetic ions form a layered square lattice. Within each layer, the local inversion symmetry is broken, but a pair of the nearest neighboring two layers enjoy the inversion symmetry. The golden arrows represent the spin orbit coupling vectors.

Hamiltonian for each layer is assumed to be

$$\mathcal{H}_l = -t \sum_{\langle i,j \rangle, \alpha} c_{il\alpha}^\dagger c_{jl\alpha} - i\lambda \sum_{\langle i,j \rangle, \alpha\beta} c_{il\alpha}^\dagger \sigma_{\alpha\beta} \cdot (-1)^l \mathbf{d}_{ij} c_{jl\beta} + \text{H.C.} - \frac{J_H}{2} \sum_{i, \alpha\beta} c_{il\alpha}^\dagger \sigma_{\alpha\beta} c_{il\beta} \cdot \mathbf{S}_{il}. \quad (1)$$

Here i, j are site indices of the square lattice at each layer l . We consider nearest-neighboring hopping between electrons described by the creation operator $c_{il\alpha}^\dagger$ with spin index α . We have assumed a local exchange coupling between the classical spin \mathbf{S}_{il} with $|\mathbf{S}_{il}| = 1$ and the electron spin. λ is the strength of the Rashba spin orbit interaction characterized by a unit vector $(-1)^l \mathbf{d}_{ij}$ that reverses its direction from layer to layer. The unit vector is perpendicular to the bond for the Rashba spin orbit interaction $\mathbf{d}_{ij} = \hat{z} \times \mathbf{r}_{ij}/|\mathbf{r}_{ij}|$ with $\mathbf{r}_{ij} = \mathbf{r}_i - \mathbf{r}_j$. We assume a hopping between electrons in the nearest layers only when the site is aligned and neglect the interlayer spin orbit coupling (the interlayer spin orbit coupling is allowed even when there exists an inversion center),

$$\mathcal{H}_c = -t_c \sum_{i,l} c_{il+1\alpha}^\dagger c_{il\alpha} + \text{H.C.} \quad (2)$$

The total Hamiltonian $\mathcal{H}_T = \mathcal{H}_c + \sum_l \mathcal{H}_l$ is invariant under inversion transformation, which flips the even and odd layers, i.e. $l \leftrightarrow l+1$. The coupling of the localized spin \mathbf{S}_{il} with the conduction

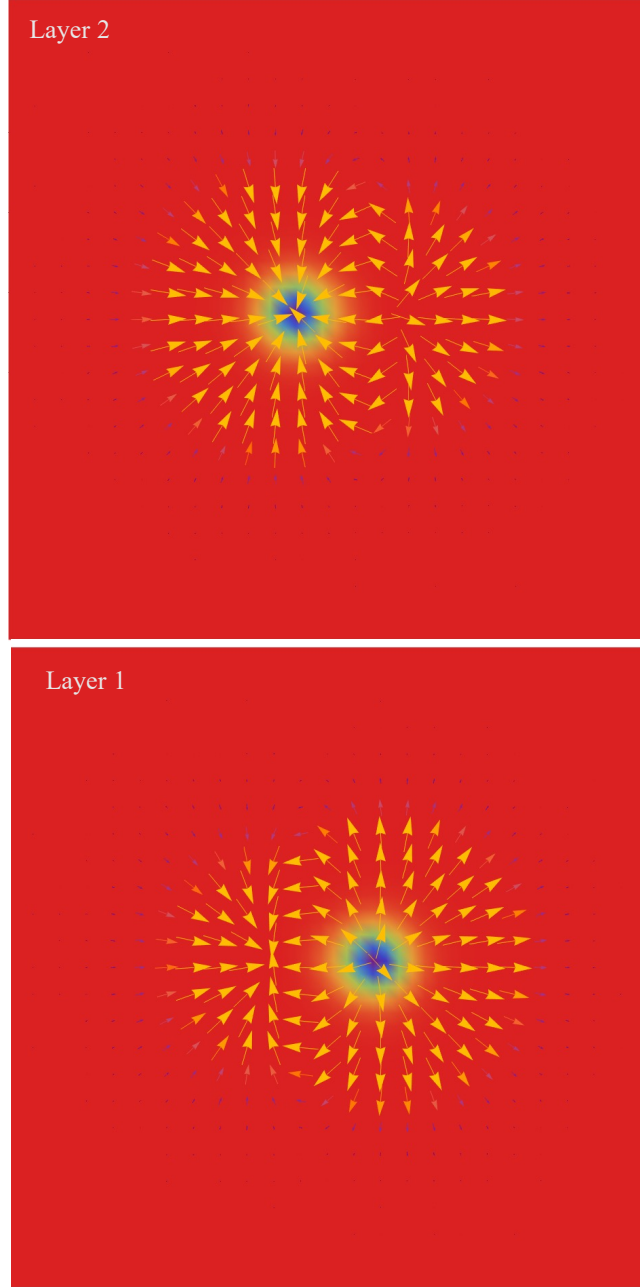


FIG. 2. Spin configuration of a skyrmion pair. Color represents out-of-plane component of spin (blue: -1 and red: +1) and arrows denote the in-plane component. There is a relative shift between the two skyrmions in a skyrmion pair. Meanwhile, a skyrmion in one layer induced a halo in its neighboring layers. Here $B = 1.0$ and $J_{12} = 0.4$.

electrons mediates an effective magnetic interaction between \mathbf{S}_{il} . In the strong coupling limit $J_H \gg t$, t_c (double-exchange mechanism), we can consider two site problem with $i = 1, 2$. [25] For \mathbf{S}_{il} in the same layer, by performing SU(2) rotation in the spin space, i.e. $\tilde{c}_{1l\alpha} = [\exp(-i\theta\boldsymbol{\sigma} \cdot (-1)^l \mathbf{d}_{12})/2]_{\alpha\beta} c_{1l\beta}$ and $\tilde{c}_{2l\alpha} = [\exp(i\theta\boldsymbol{\sigma} \cdot (-1)^l \mathbf{d}_{12})/2]_{\alpha\beta} c_{2l\beta}$ with $\tan\theta = \lambda/t$, the spin orbit coupling can be absorbed into an effective hopping parameter. The localized moment after the rotation is given by

$$\tilde{\mathbf{S}}_{1l} = \cos\theta\mathbf{S}_1 - \sin\theta(\mathbf{S}_{1l} \times (-1)^l \mathbf{d}_{12}) + (1 - \cos\theta)(\mathbf{S}_{1l} \cdot \mathbf{d}_{12})\mathbf{d}_{12}). \quad (3)$$

For $\tilde{\mathbf{S}}_{2l}$, we need to replace $\theta \rightarrow -\theta$ in the above equation. After the SU(2) rotation, the Hamiltonian is the same as the Anderson-Hasegawa Hamiltonian without a spin orbit coupling [26], and then we obtain the interaction between $\tilde{\mathbf{S}}_{il}$, $\mathcal{H} = -\kappa\tilde{t}\sqrt{1 + \tilde{\mathbf{S}}_{1l} \cdot \tilde{\mathbf{S}}_{2l}/2}$, where $\tilde{t} \equiv \sqrt{t^2 + \lambda^2}$ and κ is a constant depending on the electron density. In terms of the original classical spin \mathbf{S}_{il} , the Hamiltonian becomes

$$\mathcal{H} = -J \sum_{\langle i,j \rangle, l} \mathbf{S}_{il} \cdot \mathbf{S}_{jl} - J_{12} \sum_{i,l} \mathbf{S}_{il+1} \cdot \mathbf{S}_{il} - \sum_{\langle i,j \rangle, l} \mathbf{D}_{ij} \cdot \mathbf{S}_{il} \times \mathbf{S}_{jl} - A \sum_{i,l} (S_{il}^x S_{i+\hat{y}l}^x + S_{il}^y S_{i+\hat{x}l}^y). \quad (4)$$

Here $J = \tilde{t}\kappa\cos(2\theta)$, the compass anisotropy strength $A = \tilde{t}\kappa(1 - \cos(2\theta))$ and the interlayer coupling strength $J_{12} = t_c\kappa$. \hat{x} , \hat{y} , \hat{z} are unit vectors in the x , y , z direction, respectively. The DMI vector is perpendicular to the bond with $\mathbf{D}_{i,i+\hat{x}} = \tilde{t}\kappa\sin\theta\hat{y}$ and $\mathbf{D}_{i,i+\hat{y}} = -\tilde{t}\kappa\sin\theta\hat{x}$ (see Fig. 1). For realistic material parameters, $\lambda \ll t$, we have $J \gg |\mathbf{D}_{ij}| \gg A$. The DMI is non-perturbative because any weak DMI turns the ferromagnetic (FM) state into a magnetic spiral state, hence it should not be neglected even though it is weak. In the following discussion, we will neglect the A term. The same form of \mathcal{H} can also be derived for the superexchange mechanism [25], which is at work in Mott insulators. For the RKKY interaction valid in the region $J_H \ll t$, there appears a long range interaction between localized moments. In view of the broad relevance of the Hamiltonian Eq. (4), we will treat J_{12} as a free parameter which can be antiferromagnetic (AFM) or FM. For $|\mathbf{D}_{ij}|/J \ll 1$, the relevant length scale of the possible spin textures is much longer than the atomic (or tight-binding) lattice parameter. We can write Eq. (4) in the continuum limit

$$\mathcal{H} = \sum_l \int dr^2 \left[\frac{J}{2} (\nabla \mathbf{S}_l)^2 + D(-1)^l [S_z(\nabla \cdot \mathbf{S}) - (\mathbf{S} \cdot \nabla)S_z] - J_{12} \mathbf{S}_l \cdot \mathbf{S}_{l+1} - \mathbf{B} \cdot \mathbf{S}_l \right], \quad (5)$$

where we have included a Zeeman coupling to spins and D is the magnitude of DMI. When $J_{12} = 0$, Eq. (5) reduces two copies of the well-studied Hamiltonian for chiral magnets, which supports both single skyrmion and skyrmion lattice solutions. The spin texture depends on the

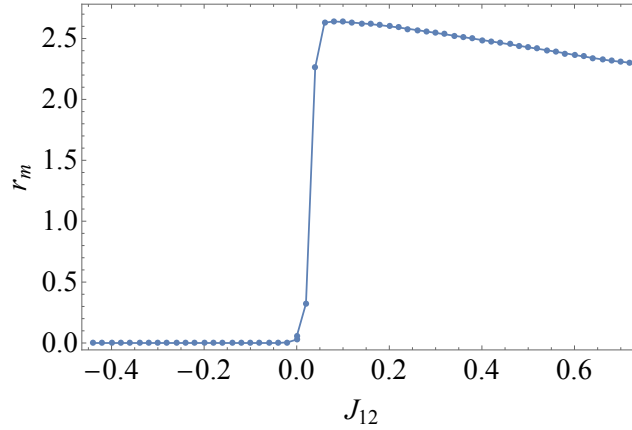


FIG. 3. Optimal relative separation between the two skyrmions in a skyrmion pair obtained by numerical minimizing of the energy. The skyrmion pair becomes unstable when J_{12} is outside of the range plotted in the figure. Here $B = 1.0$.

form of the DMI. In our case, the skyrmion is of Néel type. In one layer, the in-plane component of the spins of a skyrmion is pointing outward along the radial direction of the skyrmion while in the other layer, the spins are pointing inward, see Fig. 2 for an example. The former skyrmion has helicity 0 and the latter has helicity π . Such a spin configuration costs energy in interlayer coupling J_{12} , regardless of whether it is AFM or FM. Our task is to understand the behavior of a single skyrmion metastable state in the ferromagnetic background and the skyrmion lattice in the presence of a nonzero J_{12} . In the following, we will take the two dimensional limit by keeping minimal two layers in Eq. (5). We will use a dimensionless unit by normalizing length in unit of J/D and energy in unit of J^2/D . The model has two independent parameters B and J_{12} , both of which are in units of D^2/J .

III. SINGLE SKYRMION SOLUTION

Let us first study the properties and dynamics of a skyrmion pair in a ferromagnetic background, with one skyrmion sitting in the top layer and the other skyrmion sitting in the bottom layer. The top and bottom layers are related by the inversion symmetry. The spins away from the skyrmion center are fully polarized by the magnetic field, which requires B to be much larger than $|J_{12}|$ if $J_{12} < 0$. We minimize the energy numerically with a skyrmion pair as an initial condition. The two skyrmions in the skyrmion pair form a bound state with attraction between the two skyrmions.

The relative shift of the two skyrmions depends on J_{12} . For $J_{12} < 0$ (AFM interlayer coupling), the two skyrmions in different layers sit on top of each other. While for $J_{12} > 0$ (FM interlayer coupling), there is a relative shift between the two skyrmions and the relative shift increases with $|J_{12}|$, see Fig. 3. When there is a relative shift, the skyrmion in one layer couples to the otherwise ferromagnetic state in the neighboring layer and generates a shadow spin texture with winding of spins, as displayed in Fig. 2. The reason why the two skyrmions in two layers shift from each other for $J_{12} > 0$ can be understood as follows. Due to the opposite helicity of the two skyrmions, the in-plane component of the spins associated with the two skyrmions is opposite in the two layers, which is favored by $J_{12} < 0$. For $J_{12} > 0$, the two skyrmions avoid sitting atop each other to save cost in the ferromagnetic coupling between the in-plane component of spins. The out-of-plane component of spins is less important in determining the relative position of skyrmions because the Zeeman coupling dominates over other interactions.

To quantify the shape of the skyrmion pair, we introduce the skyrmion topological charge center for a skyrmion in the l -th layer

$$\mathbf{r}_l = \int_{l\text{-th layer}} d\mathbf{r}^2 \mathbf{r}_l \mathbf{S}_l \cdot \partial_x \mathbf{S}_l \times \partial_y \mathbf{S}_l / \int_{l\text{-th layer}} d\mathbf{r}^2 \mathbf{S}_l \cdot \partial_x \mathbf{S}_l \times \partial_y \mathbf{S}_l \quad (6)$$

and the relative shift $r_{12} = |\mathbf{r}_1 - \mathbf{r}_2|$. The optimal r_{12} (denoted as r_m) that minimizes the skyrmion pair energy as a function of J_{12} is shown in Fig. 3. The separation between the two skyrmions quickly saturates to a value and then slowly decreases as J_{12} increases. The skyrmion pair becomes unstable when $J_{12} > 0.72$ or $J_{12} < -0.44$ at $B = 1.0$.

Now we turn to the dynamics of the skyrmion pair. We consider both the spin transfer torque and the spin Hall torque. The dynamics of spin is given by

$$\partial_t \mathbf{S} = -\gamma \mathbf{S} \times \mathbf{H}_{\text{eff}} + \alpha \mathbf{S} \times \partial_t \mathbf{S} + \boldsymbol{\tau}, \quad (7)$$

where $\mathbf{H}_{\text{eff}} \equiv -\delta \mathcal{H} / \delta \mathbf{S}$ is an effective field, α is the Gilbert damping and γ is the gyromagnetic ratio. We use $\alpha = 0.2$ in simulations. The torque is $\boldsymbol{\tau} = \frac{\hbar \gamma}{2e} (\mathbf{J} \cdot \nabla) \mathbf{S}$ for the spin transfer torque [27, 28] and $\boldsymbol{\tau} = \frac{\hbar \gamma \theta_{\text{sh}}}{2ed} \mathbf{S} \times [\mathbf{S} \times (\hat{\mathbf{z}} \times \mathbf{J})]$ for the spin Hall torque [29–31]. Here θ_{sh} is the spin Hall angle, d is the film thickness and $e > 0$ is the elementary electric charge. For a weak drive, the deformation of the skyrmion is negligible [32] and the skyrmion dynamics is described by its translational motion in space, which is a Goldstone mode in a clean system. The translational motion is parameterized by the skyrmion center \mathbf{R}_l and the corresponding velocity $\mathbf{v}_l = \dot{\mathbf{R}}_l$, which obey the Thiele's equation [33]. For the spin transfer torque, Thiele's equation for the two skyrmions in

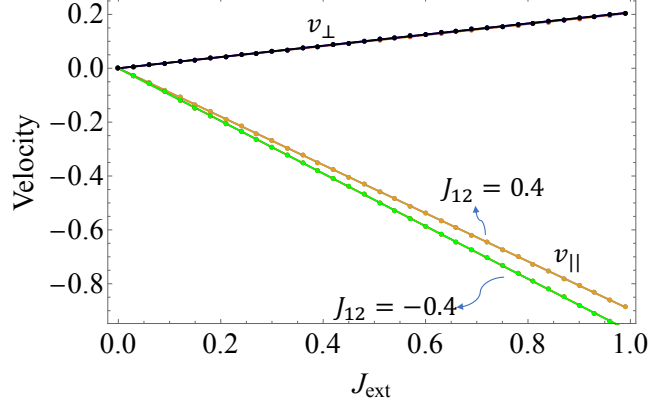


FIG. 4. Skyrmion dynamics under a spin transfer torque. The two skyrmions in a skyrmion pair move as a whole, and move almost anti-parallel to the applied current direction with a small transverse velocity proportional to the damping constant. The velocity vs J_{ext} for $J_{12} < 0$ is the same as that for $J_{12} = 0$ within numerical resolution. The velocity at a given J_{ext} becomes smaller when $J_{12} > 0$ is increased due to the induced shadow texture in the neighboring layer. Here $B = 1.0$ and time is in unit of $J/(\gamma D^2)$.

a skyrmion pair reads

$$Q_l \hat{z} \times \left(\mathbf{v}_l + \frac{\hbar \gamma}{2e} \mathbf{J}_{\text{ext}} \right) = -\alpha \eta_l \mathbf{v}_l + (-1)^l \mathbf{F}_{12}, \quad (8)$$

where \mathbf{F}_{12} is the attraction between the two skyrmions at two layers. Here η_l is the skyrmion form factor $\eta_l \equiv \int_{l\text{-th layer}}' (\partial_\mu \mathbf{S}_l)^2 dr^2 / (4\pi)$ and the skyrmion topological charge $Q_l = \int_{l\text{-th layer}}' dr^2 \mathbf{S}_l \cdot \partial_x \mathbf{S}_l \times \partial_y \mathbf{S}_l / (4\pi)$, where the integration is restricted to the region around a skyrmion. [34] The Thiele's equation for the spin transfer torque does not depend on the helicity of the skyrmions and hence the two skyrmions respond to the spin transfer torque in the same way. The two skyrmions move as a whole skyrmion pair almost the same as those in the decoupled limit $J_{12} = 0$. The skyrmion pair velocity can be found in $v_{\parallel} = -\hbar Q^2 J_{\text{ext}} / [2e(Q^2 + \alpha^2 \eta^2)]$ and $v_{\perp} = -\hbar \alpha \eta Q J_{\text{ext}} / [2e(Q^2 + \alpha^2 \eta^2)]$, where v_{\parallel} (v_{\perp}) is the skyrmion velocity component parallel (perpendicular) to the current. We have approximated $\eta = \eta_l$ and $Q = Q_l$. The numerical results are shown in Fig. 4. The interlayer coupling J_{12} enters the equation through the form factor η_l because J_{12} causes a skyrmion deformation (see Fig. 2). For $J_{12} > 0$, there is a relative shift between the two skyrmions and induced shadow in the neighboring layers. As a consequence η_l for $J_{12} > 0$ is larger than these for $J_{12} \leq 0$. This explains the result in Fig. 4, where $|v_{\parallel}|$ for $J_{12} = 0.4$ is smaller than that for $J_{12} = -0.4$.

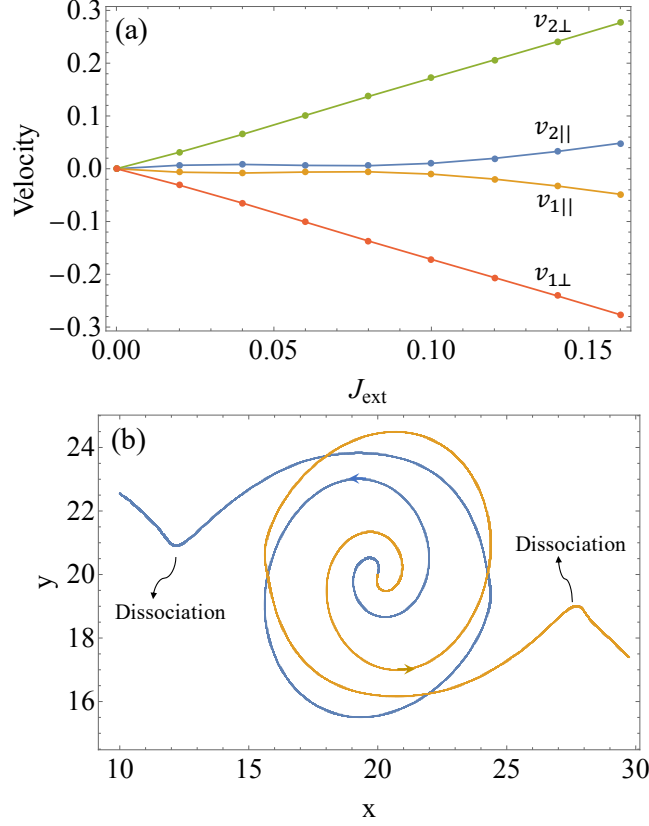


FIG. 5. (a) Velocity of the two skyrmions after a skyrmion pair disassociates at the threshold current $J_{\text{ext}}^c = 0.0085$ for $B = 1.0$ and $J_{12} = -0.4$. The two skyrmions travel in the opposite direction. (b) Trajectory of the two skyrmions in a skyrmion pair subjected to a spin Hall torque. Initially the two skyrmions are sitting atop of each other for $J_{12} = -0.4$. The point when the skyrmion pair disassociates is indicated in the figure.

The dynamics of skyrmion pair driven by the spin Hall torque is more interesting because the spin Hall torque couples to the helicity. [35] The Thiele's equation in this case is

$$Q_l \hat{z} \times \mathbf{v}_l + \alpha \eta_l \mathbf{v}_l = \frac{\hbar \gamma \theta_{\text{sh}}}{2ed} J_{\text{ext}} \mathbf{Y}_l + (-1)^l \mathbf{F}_{12}, \quad (9)$$

$Y_{l,\mu} = (\hat{z} \times \hat{\mathbf{J}}_{\text{ext}}) \cdot \int_{1-\text{th layer}}' (\partial_\mu \mathbf{S}_l \times \mathbf{S}_l) dr^2 / (4\pi)$ with $\mu = x, y$. $\hat{\mathbf{J}}_{\text{ext}}$ is a unit vector along the current direction. It is straightforward to verify $Y_{1,\mu} = -Y_{2,\mu}$ when the two skyrmions have opposite helicity. Therefore, the two skyrmions in a skyrmion pair tend to move in a different trajectory. For Néel skyrmions with helicity equal to 0 or π , \mathbf{Y}_l is parallel to the current direction and its magnitude is denoted by $Y_{l\parallel}$. When the current is small, the force F_{12} balances the different driving forces acting on the two skyrmions by adjusting the relative shift of position between the

two skyrmions. The corresponding solution is $\mathbf{v}_l = 0$ and $|F_{12}| = |\frac{\hbar\gamma\theta_{\text{sh}}}{2ed}J_{\text{ext}}\mathbf{Y}_l|$, when the current reaches a threshold, the maximal force F_{12} between the two skyrmions is no longer sufficient to cancel the disparity in the driving force between the two skyrmions. As a result, the skyrmion pair disassociates, and the two skyrmions move independently. One can obtain the skyrmion velocities by setting $F_{12} = 0$ in Eq. (9), which yields $v_{1\perp} = -QY_{1\parallel}\hbar\gamma\theta_{\text{sh}}J_{\text{ext}}/[2ed(Q^2 + (\alpha\eta)^2)]$ and $v_{1\parallel} = \alpha\eta Y_{1\parallel}\hbar\gamma\theta_{\text{sh}}J_{\text{ext}}/[2ed(Q^2 + (\alpha\eta)^2)]$, and similarly for \mathbf{v}_2 . Because $Y_{1,\mu} = -Y_{2,\mu}$, the two skyrmions move in the opposite direction, see Fig. 5 (a). The skyrmions travel almost perpendicularly to the current direction, $v_{1\perp} \gg v_{1\parallel}$.

Let us examine the dynamical process of decoupling of the two skyrmions in a skyrmion pair. We take $J_{12} < 0$ such that two skyrmions sit on top of each other. We then turn on the current and calculate \mathbf{r}_l . The trajectory is shown in Fig. 5 (b). As the current is turned on, the two skyrmions move away from each other. The trajectory is spiral due to the Magnus force $\sim \hat{\mathbf{z}} \times \mathbf{v}_l$, which forces the skyrmion to move perpendicularly to the force direction. When the skyrmion separation exceeds a threshold value, the two skyrmions decouple.

Interestingly, one can estimate $F_{12}(r)$ and hence the potential $U(r)$ from Eq. (9). This can be done in two different ways. In the first approach, one considers the static limit for a small current. Then $F_{12}(r_m) = |\frac{\hbar\gamma\theta_{\text{sh}}}{2ed}J_{\text{ext}}\mathbf{Y}_l|$ where r_m is the equilibrium relative distance between the two skyrmions. In the second approach, one directly calculates $F_{12}(r)$ from the trajectory of two skyrmions by switching on current.

It is also interesting to ask whether the internal force F_{12} produces an effective mass for the skyrmion pair, which causes a retarded response to the external drive. The answer is no. This can be seen from Eqs. (8) or (9) by rewriting the equation of motion in terms of relative coordinate $\mathbf{R}_{12} = \mathbf{R}_1 - \mathbf{R}_2$ and center of mass coordinate $\mathbf{R} = \mathbf{R}_1 + \mathbf{R}_2$. No term of the form $M\ddot{\mathbf{R}} + \dots = \mathbf{F}_{\text{ext}}$ with \mathbf{F}_{ext} being a driving force, is generated, hence the mass generation due to \mathbf{F}_{12} is absent. However, the skyrmion mass can be generated through excitation of high energy internal modes [32, 36, 37], which has been neglected here.

IV. SKYRMION LATTICE

We then determine the equilibrium phase diagram of the Hamiltonian Eq. (5) in two dimensions. We perform numerical annealing from high temperature disordered state to zero temperature and determine the ground state spin configuration. We discretize Eq. (5) into a square lattice with

a lattice parameter $dr = 0.8$, such that the magnetic spiral at $B = 0$ and $J_{12} = 0$ has roughly 8 lattice parameters. The phase diagram is shown in Fig. 6 where the triangular lattice of the skyrmion pair is stabilized in a wide region in the B and J_{12} space. A large value of $|J_{12}|$ disfavors the skyrmion crystal. When stabilized, the skyrmion crystal is more stable for an AFM J_{12} than that for an FM J_{12} . The skyrmion crystal is aligned in the direction perpendicular to the layers when $J_{12} < 0$. While for $J_{12} > 0$, the in-plane position of the skyrmions is located at positions corresponding to the interstitial sites of the skyrmion lattice in the nearest neighboring layers. As such a relative shift is not always optimal for a skyrmion pair (see Fig. 2), this explains why the skyrmion crystal is less favorable for $J_{12} > 0$ than that for $J_{12} < 0$. Typical spin configurations obtained from numerical calculations are presented in Figs. 7 and 8. It is clear that the skyrmion has opposite helicity between the nearest neighbor layers. In addition to the skyrmion lattice phase, the standard magnetic spiral state is stabilized in the low magnetic field region and the spins are fully polarized at high magnetic fields.

Very recently, lattice spin Hamiltonian which reduces to Eq. (5) in the continuum limit by taking the ordering wave vector $q \rightarrow 0$ was studied by Hayami [38]. Our phase diagram differs from that in Ref. [38], where more 3- Q states have been identified in addition to the skyrmion lattice phase. One possible reason for the discrepancy is due to the underlying spin lattice symmetry. In Ref. [38], spins are defined on triangular lattice with $q = \pi/3$, while in the present work, we discretize the continuum model into a square lattice with a fine mesh to minimize the discretization effect. Our method reproduces the known results well when $J_{12} = 0$. The spin lattice generates a potential to orient the spin modulation wavevector, which can be quite different for the triangular and square lattice for a relatively large q . It is known from the previous study [39] that the underlying spin lattice symmetry can have profound consequences on the spin textures that can be realized. In Ref. [38], Hayami restricted to the six in-plane wave vectors \mathbf{q}_i with $|\mathbf{q}_i| = \pi/3$ that are related by six-fold rotation in the simulations. This may also be a source of the discrepancy. In contrast, we have taken into account all the qs permitted by discretization in our numerical calculations.

V. DISCUSSION AND SUMMARY

Here we discuss the dynamics of skyrmion lattice in the presence of a spin Hall torque. When the current is large such that the skyrmion lattice in two layers both depins from impurities and

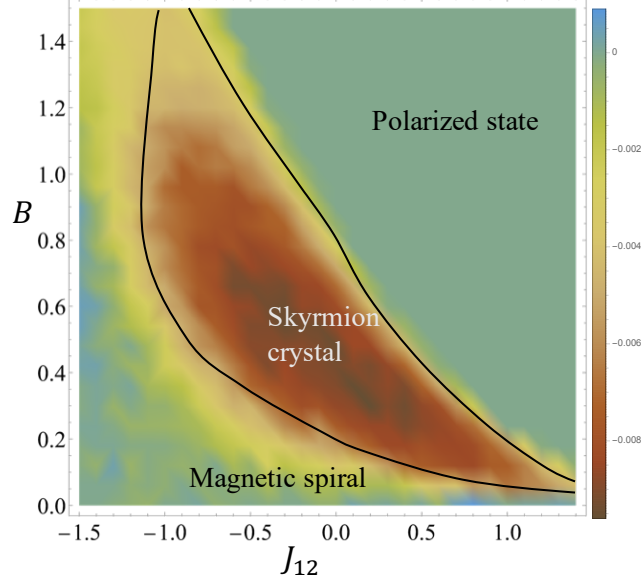


FIG. 6. Phase diagram of the model Eq. (5) in two dimensions (minimal two layers limit). The color represents the skyrmion density. The triangular skyrmion lattice is stabilized in a wide region in the parameter space of J_{12} and B . The phase boundary is constructed based on magnetization, skyrmion topological density and their derivatives as a function of J_{12} and B . The system size is 40×40 and the periodic boundary condition is used.

decouples from each other, the two skyrmion lattices move in the opposite direction. If we take the skyrmion lattice in one layer as a reference, then effectively the skyrmion lattice in the other layer experiences a periodic potential produced by the reference skyrmion lattice. This produces an oscillating component in the skyrmion lattice velocity with period $T_v \propto a_L/v_{12}$ where a_L is the skyrmion lattice parameter and v_{12} is the relative velocity. In the presence of conduction electrons, the coupling between the skyrmion lattice and conduction electrons generates an oscillating emergent electric field. [40] It is known in the case of the Abrikosov vortex lattice that driving the vortex lattice with an ac current in addition to a dc current produces Shapiro steps when the frequency associated with the periodic passing of the vortex lattice through pinning sites is commensurate with the ac current frequency. [41, 42] Here similarly phenomenology is expected when the skyrmion lattice is driven through defects. No ac current is required in this case because the relative motion of the two skyrmion lattices already provides an oscillating velocity component. The situation is similar to the fractional vortex lattice in multicomponent superconductors discussed in Ref. [43], with a notable difference that the Magnus force is dominant over the viscous

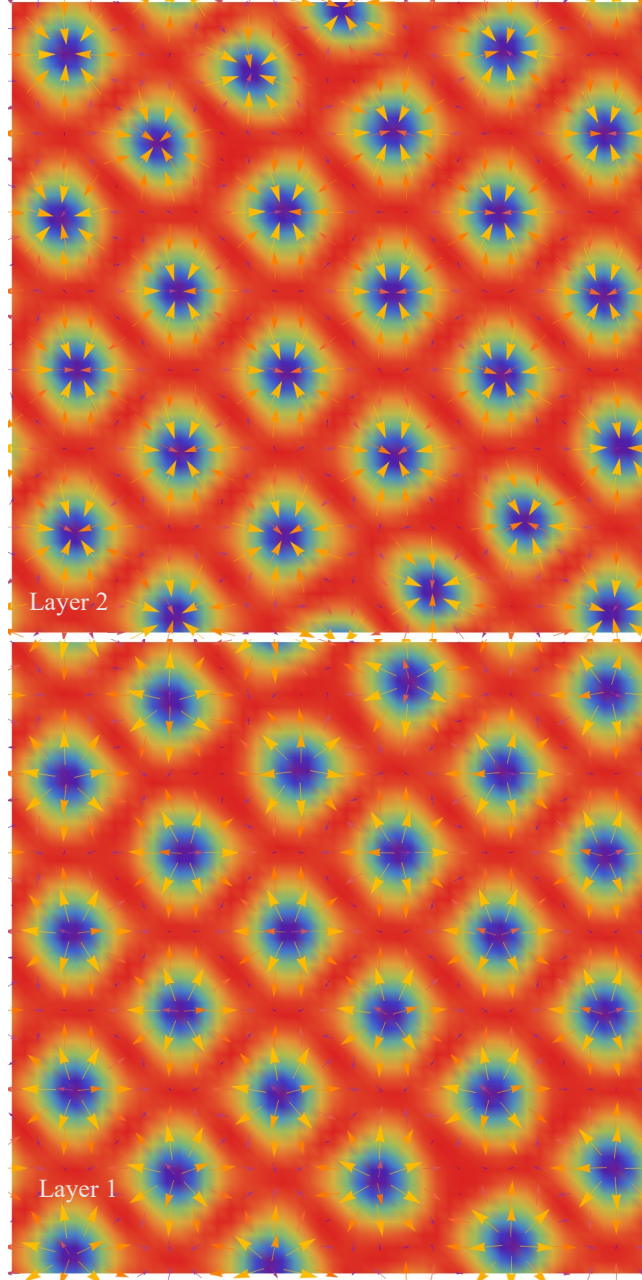


FIG. 7. Skyrmion lattice configuration in the neighboring two layers for $J_{12} = 0.6$ and $B = 0.24$. The skyrmion lattice in one layer is sitting at the interstitial sites of the neighboring layer, and with an opposite helicity. Here color represents out-of-plane component of spin (blue: -1 and red: +1) and arrows denote the in-plane component. The system size is 40×40 and the periodic boundary condition is used.

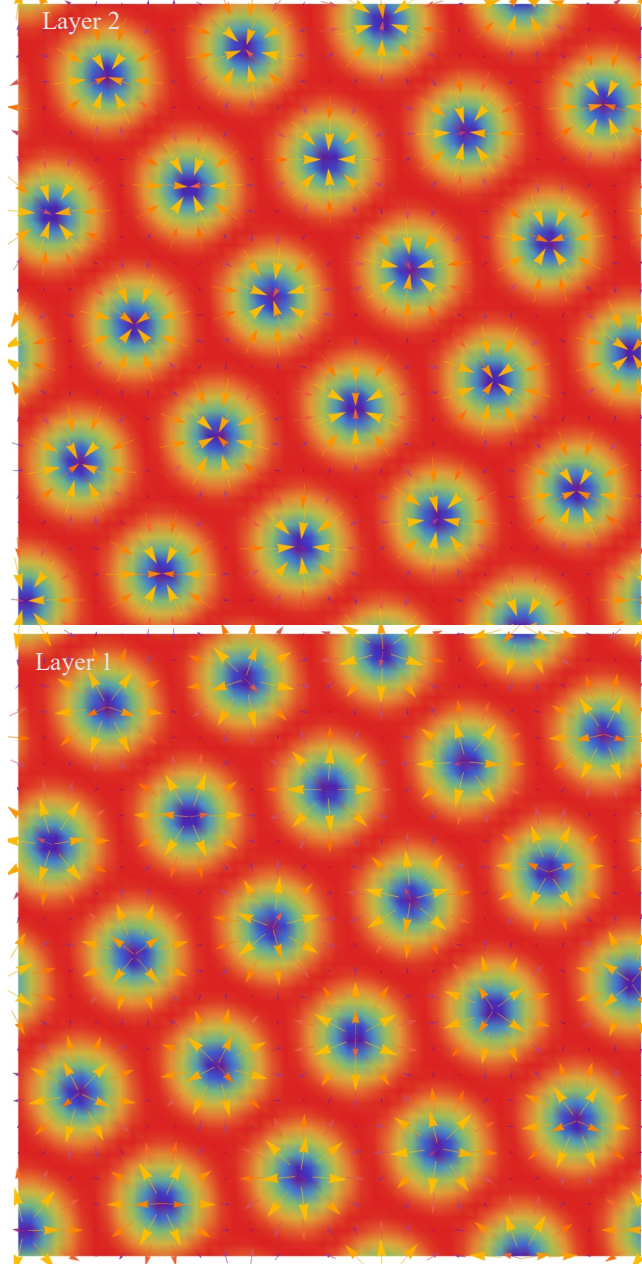


FIG. 8. Skyrmion lattice configuration in the neighboring two layers for $J_{12} = -0.5$ and $B = 0.9$. The skyrmion lattices in the two layers are aligned, and with an opposite helicity. Here color represents out-of-plane component of spin (blue: -1 and red: +1) and arrows denote the in-plane component. The system size is 40×40 and the periodic boundary condition is used.

force for the dynamics of skyrmions.

We then discuss some open questions for future studies. One direct extension of the current work is the phase diagram in three dimensions. It is known that the magnetic phase diagram in two and three dimensions differs radically for chiral magnets [5, 6, 44], and we expect that the same is also true here. Here, we have neglected the interlayer spin orbit coupling. If such a spin orbit coupling is taken into account, there can be an extra twist of spins along the direction perpendicular to layers. This can generate three dimensional skyrmion texture with different skyrmion lattice symmetry. This idea has been validated in three dimensional inversion symmetric magnets with frustrated interlayer couplings [45]. Going beyond the simple spin orbit coupling vectors and local DMI vector distribution studied here, more complex local DMI vector distributions are possible depending on the local inversion symmetry breaking pattern, atomic crystal structure, and constrained by Moriya's rule [15], which is likely to generate a plethora of spin textures for spins sitting at different sub-lattices.

To summarize, we demonstrate that there exists a skyrmion lattice in centrosymmetric magnets with a local inversion symmetry breaking. The lack of local inversion symmetry allows for a local DMI which is sufficient to stabilize the skyrmion spin texture. For the particular crystal structure considered here, the DMI in the nearest neighboring layer has an alternating sign and the skyrmion in the neighboring layers has opposite helicity. The dynamics of skyrmions can be quite different when the external drive, such as spin Hall torque, couples to the helicity of the skyrmions. We have determined the equilibrium skyrmion lattice phase diagram and demonstrated the stability of the skyrmion lattice against the interlayer coupling. The skyrmion with alternating helicity in different layers can be detected experimentally using standard imaging methods, such as neutron scattering spectroscopy and Lorentz transmission electron microscopy imaging at a surface with a controlled layer termination. The skyrmions at different layers have the same topological charge and therefore give rise to the topological Hall effect when they couple to conduction electrons, which can be measured experimentally. The local DMI mechanism identified here is expected to have broader implications in determining spin textures in centrosymmetric magnets, which has largely been overlooked so far. Our results point to a new direction to search for skyrmions in magnetic materials.

VI. ACKNOWLEDGEMENTS

The work was carried out under the auspices of the U.S. DOE NNSA under contract No. 89233218CNA000001 through the LDRD Program, and was performed, in part, at the Center for Integrated Nanotechnologies, an Office of Science User Facility operated for the U.S. DOE Office of Science, under user proposals #2018BU0010 and #2018BU0083. Computer resources for numerical calculations were supported by the Institutional Computing Program at LANL.

Note added– We have become aware of a recent manuscript [38], which has some overlap with the current work. Recent neutron scattering measurement of centrosymmetric CeAgBi₂ points to the existence of the skyrmion lattice stabilized by the mechanism discussed here. [46] The CeAgBi₂ unit cell contains two Ce with an inversion center locating at the bond center. For each Ce, the inversion symmetry is broken locally.

-
- [1] Naoto Nagaosa and Yoshinori Tokura, “Topological properties and dynamics of magnetic skyrmions,” [Nature Nanotechnology](#) **8**, 899–911 (2013).
 - [2] Roland Wiesendanger, “Nanoscale magnetic skyrmions in metallic films and multilayers: a new twist for spintronics,” [Nature Reviews Materials](#) **1**, 1–11 (2016).
 - [3] Albert Fert, Nicolas Reyren, and Vincent Cros, “Magnetic skyrmions: advances in physics and potential applications,” [Nature Reviews Materials](#) **2**, 1–15 (2017).
 - [4] Wanjun Jiang, Gong Chen, Kai Liu, Jiadong Zang, Suzanne G. E. te Velthuis, and Axel Hoffmann, “Skyrmions in magnetic multilayers,” [Physics Reports Skyrmions in Magnetic Multilayers](#), **704**, 1–49 (2017).
 - [5] S. Mühlbauer, B. Binz, F. Jonietz, C. Pfleiderer, A. Rosch, A. Neubauer, R. Georgii, and P. Böni, “Skyrmion lattice in a chiral magnet,” [Science](#) **323**, 915 (2009).
 - [6] X. Z. Yu, Y. Onose, N. Kanazawa, J. H. Park, J. H. Han, Y. Matsui, N. Nagaosa, and Y. Tokura, “Real-space observation of a two-dimensional skyrmion crystal,” [Nature](#) **465**, 901 (2010).
 - [7] S. Seki, X. Z. Yu, S. Ishiwata, and Y. Tokura, “Observation of skyrmions in a multiferroic material,” [Science](#) **336**, 198 (2012).
 - [8] Ajaya K. Nayak, Vivek Kumar, Tianping Ma, Peter Werner, Eckhard Pippel, Roshnee Sahoo, Franoise Damay, Ulrich K. Rößler, Claudia Felser, and Stuart S. P. Parkin, “Magnetic antiskyrmions above

- room temperature in tetragonal Heusler materials,” [Nature](#) **548**, 561 (2017).
- [9] Stefan Heinze, Kirsten von Bergmann, Matthias Menzel, Jens Brede, André Kubetzka, Roland Wiesendanger, Gustav Bihlmayer, and Stefan Blügel, “Spontaneous atomic-scale magnetic skyrmion lattice in two dimensions,” [Nature Physics](#) **7**, 713–718 (2011).
- [10] Niklas Romming, Christian Hanneken, Matthias Menzel, Jessica E. Bickel, Boris Wolter, Kirsten von Bergmann, André Kubetzka, and Roland Wiesendanger, “Writing and deleting single magnetic skyrmions,” [Science](#) **341**, 636–639 (2013).
- [11] Takashi Kurumaji, Taro Nakajima, Max Hirschberger, Akiko Kikkawa, Yuichi Yamasaki, Hajime Sagayama, Hironori Nakao, Yasujiro Taguchi, Taka-hisa Arima, and Yoshinori Tokura, “Skyrmion lattice with a giant topological Hall effect in a frustrated triangular-lattice magnet,” [Science](#) (2019), [10.1126/science.aau0968](#).
- [12] Nguyen Duy Khanh, Taro Nakajima, Xiuzhen Yu, Shang Gao, Kiyohi Shibata, Max Hirschberger, Yuichi Yamasaki, Hajime Sagayama, Hironori Nakao, Licong Peng, Kiyomi Nakajima, Rina Takagi, Taka-hisa Arima, Yoshinori Tokura, and Shinichiro Seki, “Nanometric square skyrmion lattice in a centrosymmetric tetragonal magnet,” [Nature Nanotechnology](#) **15**, 444–449 (2020).
- [13] Max Hirschberger, Taro Nakajima, Shang Gao, Licong Peng, Akiko Kikkawa, Takashi Kurumaji, Markus Kriener, Yuichi Yamasaki, Hajime Sagayama, Hironori Nakao, Kazuki Ohishi, Kazuhisa Kakurai, Yasujiro Taguchi, Xiuzhen Yu, Taka-hisa Arima, and Yoshinori Tokura, “Skyrmion phase and competing magnetic orders on a breathing kagomé lattice,” [Nature Communications](#) **10**, 5831 (2019).
- [14] I. Dzyaloshinsky, “A thermodynamic theory of weak ferromagnetism of antiferromagnetics,” [J. Phys. Chem. Solids](#) **4**, 241 (1958).
- [15] Tôru Moriya, “Anisotropic superexchange interaction and weak ferromagnetism,” [Phys. Rev.](#) **120**, 91 (1960).
- [16] Tôru Moriya, “New mechanism of anisotropic superexchange interaction,” [Phys. Rev. Lett.](#) **4**, 228–230 (1960).
- [17] A. N. Bogdanov and D. A. Yablonskii, “Thermodynamically stable “vortices” in magnetically ordered crystals: The mixed state of magnets,” [Sov. Phys. JETP](#) **68**, 101 (1989).
- [18] A. Bogdanov and A. Hubert, “Thermodynamically stable magnetic vortex states in magnetic crystals,” [J. Magn. Magn. Mater.](#) **138**, 255 – 269 (1994).

- [19] U. K. Rößler, A. N. Bogdanov, and C. Pfleiderer, “Spontaneous skyrmion ground states in magnetic metals,” *Nature* **442**, 797 (2006).
- [20] Tsuyoshi Okubo, Sungki Chung, and Hikaru Kawamura, “Multiple- q states and the skyrmion lattice of the triangular-lattice heisenberg antiferromagnet under magnetic fields,” *Phys. Rev. Lett.* **108**, 017206 (2012).
- [21] A. O. Leonov and M. Mostovoy, “Multiply periodic states and isolated skyrmions in an anisotropic frustrated magnet,” *Nature Communications* **6**, 8275 (2015).
- [22] Shi-Zeng Lin and Satoru Hayami, “Ginzburg-landau theory for skyrmions in inversion-symmetric magnets with competing interactions,” *Phys. Rev. B* **93**, 064430 (2016).
- [23] S A Owerre, “A first theoretical realization of honeycomb topological magnon insulator,” *Journal of Physics: Condensed Matter* **28**, 386001 (2016).
- [24] “Cerh2as2 crystal structure: Datasheet from “pauling file multinaries edition – 2012” in *springer materials* (https://materials.springer.com/isp/crystallographic/docs/sd_0539528),” Copyright 2016 Springer-Verlag Berlin Heidelberg & Material Phases Data System (MPDS), Switzerland & National Institute for Materials Science (NIMS), Japan.
- [25] Sumilan Banerjee, James Rowland, Onur Erten, and Mohit Randeria, “Enhanced stability of skyrmions in two-dimensional chiral magnets with rashba spin-orbit coupling,” *Phys. Rev. X* **4**, 031045 (2014).
- [26] P. W. Anderson and H. Hasegawa, “Considerations on double exchange,” *Phys. Rev.* **100**, 675–681 (1955).
- [27] J.C. Slonczewski, “Current-driven excitation of magnetic multilayers,” *Journal of Magnetism and Magnetic Materials* **159**, L1–L7 (1996).
- [28] Gen Tatara, Hiroshi Kohno, and Junya Shibata, “Microscopic approach to current-driven domain wall dynamics,” *Phys. Rep.* **468**, 213 (2008).
- [29] Satoru Emori, Uwe Bauer, Sung-Min Ahn, Eduardo Martinez, and Geoffrey S. D. Beach, “Current-driven dynamics of chiral ferromagnetic domain walls,” *Nature Materials* **12**, 611–616 (2013).
- [30] Kwang-Su Ryu, Luc Thomas, See-Hun Yang, and Stuart Parkin, “Chiral spin torque at magnetic domain walls,” *Nature Nanotechnology* **8**, 527–533 (2013).
- [31] Luqiao Liu, Chi-Feng Pai, Y. Li, H. W. Tseng, D. C. Ralph, and R. A. Buhrman, “Spin-Torque Switching with the Giant Spin Hall Effect of Tantalum,” *Science* **336**, 555–558 (2012).

- [32] Shi-Zeng Lin, “Dynamics and inertia of a skyrmion in chiral magnets and interfaces: A linear response approach based on magnon excitations,” [Phys. Rev. B **96**, 014407 \(2017\)](#).
- [33] A. A. Thiele, “Steady-state motion of magnetic domains,” [Phys. Rev. Lett. **30**, 230–233 \(1973\)](#).
- [34] Shi-Zeng Lin, Charles Reichhardt, Cristian D. Batista, and Avadh Saxena, “Particle model for skyrmions in metallic chiral magnets: Dynamics, pinning, and creep,” [Phys. Rev. B **87**, 214419 \(2013\)](#).
- [35] Shi-Zeng Lin, “Edge instability in a chiral stripe domain under an electric current and skyrmion generation,” [Phys. Rev. B **94**, 020402 \(2016\)](#).
- [36] Imam Makhfudz, Benjamin Krüger, and Oleg Tchernyshyov, “Inertia and chiral edge modes of a skyrmion magnetic bubble,” [Phys. Rev. Lett. **109**, 217201 \(2012\)](#).
- [37] Christoph Schütte, Junichi Iwasaki, Achim Rosch, and Naoto Nagaosa, “Inertia, diffusion, and dynamics of a driven skyrmion,” [Phys. Rev. B **90**, 174434 \(2014\)](#).
- [38] Satoru Hayami, “Skyrmion crystal and spiral phases in centrosymmetric bilayer magnets with staggered dzyaloshinskii-moriya interaction,” [Phys. Rev. B **105**, 014408 \(2022\)](#).
- [39] Satoru Hayami, Shi-Zeng Lin, and Cristian D. Batista, “Bubble and skyrmion crystals in frustrated magnets with easy-axis anisotropy,” [Phys. Rev. B **93**, 184413 \(2016\)](#).
- [40] T. Schulz, R. Ritz, A. Bauer, M. Halder, M. Wagner, C. Franz, C. Pfleiderer, K. Everschor, M. Garst, and A. Rosch, “Emergent electrodynamics of skyrmions in a chiral magnet,” [Nat. Phys. **8**, 301 \(2012\)](#).
- [41] J. M. Harris, N. P. Ong, R. Gagnon, and L. Taillefer, “Washboard frequency of the moving vortex lattice in $\text{YBa}_2\text{Cu}_3\text{O}_{6.93}$ detected by ac-dc interference,” [Phys. Rev. Lett. **74**, 3684–3687 \(1995\)](#).
- [42] L. Van Look, E. Rosseel, M. J. Van Bael, K. Temst, V. V. Moshchalkov, and Y. Bruynseraede, “Shapiro steps in a superconducting film with an antidot lattice,” [Phys. Rev. B **60**, R6998–R7000 \(1999\)](#).
- [43] Shi-Zeng Lin and Charles Reichhardt, “Stabilizing fractional vortices in multiband superconductors with periodic pinning arrays,” [Phys. Rev. B **87**, 100508 \(2013\)](#).
- [44] Stefan Buhrandt and Lars Fritz, “Skyrmion lattice phase in three-dimensional chiral magnets from monte carlo simulations,” [Phys. Rev. B **88**, 195137 \(2013\)](#).
- [45] Shi-Zeng Lin and Cristian D. Batista, “Face centered cubic and hexagonal close packed skyrmion crystals in centrosymmetric magnets,” [Phys. Rev. Lett. **120**, 077202 \(2018\)](#).
- [46] W. Simeth et. al., preprint (2024).